

Journal of Materials Chemistry B

Materials for biology and medicine

Accepted Manuscript

This article can be cited before page numbers have been issued, to do this please use: P. Du, J. H. Yan, S. Long, H. xiong, N. Wen, S. Cai, Y. Wang, D. Peng, Z. Liu and Y. Liu, *J. Mater. Chem. B*, 2020, DOI: 10.1039/D0TB00489H.



This is an Accepted Manuscript, which has been through the Royal Society of Chemistry peer review process and has been accepted for publication.

Accepted Manuscripts are published online shortly after acceptance, before technical editing, formatting and proof reading. Using this free service, authors can make their results available to the community, in citable form, before we publish the edited article. We will replace this Accepted Manuscript with the edited and formatted Advance Article as soon as it is available.

You can find more information about Accepted Manuscripts in the [Information for Authors](#).

Please note that technical editing may introduce minor changes to the text and/or graphics, which may alter content. The journal's standard [Terms & Conditions](#) and the [Ethical guidelines](#) still apply. In no event shall the Royal Society of Chemistry be held responsible for any errors or omissions in this Accepted Manuscript or any consequences arising from the use of any information it contains.

Tumor Microenvironment and NIR Laser Dual Responsive Release of Berberine 9-O-pyrazole Alkyl Derivative Loaded in Graphene Oxide Nanosheets for Chemo-photothermal Synergistic Cancer Therapy

View Article Online
DOI: 10.1039/C9TB01000A

Peifang Du^a, Jianhua Yan^b, Shuo Long^a, Hongjie Xiong^b, Nachuan Wen^a, Shundong Cai^b, Yirong Wang^a, Dongming Peng^c, Zhenbao Liu^{b,e,*}, Yanfei Liu^{a,**}

a. Department of Pharmaceutical Engineering, College of Chemistry and Chemical Engineering, Central South University, Changsha, 410083, Hunan Province, P. R. China

b. Xiangya School of Pharmaceutical Sciences, Central South University, Changsha, 410013, Hunan Province, P. R. China

c. Department of Medicinal Chemistry, School of Pharmacy, Hunan University of Chinese Medicine, Changsha, 410208, Hunan Province, P. R. China

e. Molecular Imaging Research Center of Central South University, Changsha 410008, Hunan, P. R. China

*Corresponding author

** Corresponding author

Corresponding author: Zhenbao Liu

Mailing address: Central South University, No.172, Tongzipo Road, Changsha, 410013, China

Tel.: +86-731 83992279; fax: +86-731 83992279

Mobile phone: 13723886533

E-mail: zhenbaoliu@csu.edu.cn

Corresponding author: Yanfei Liu

Mailing address: *Department of Pharmaceutical Engineering, School of Chemistry and Chemical Engineering, Central South University, Changsha, 410083, Hunan Province, P. R. China*

Tel.: +86-731 88879616; fax: +86-731 88879616

Mobile phone: 13017381167

E-mail: liuyf@csu.edu.cn

Abstract: Berberine 9-O-pyrazole alkyl derivative, a chemical compound B3 previously synthesized by our group, showed anti-cancer activity. However, B3 lacks targeting cytotoxicity to cancer cells, leading to obvious toxic side effects on normal cells. To solve this problem, here, we prepared a drug delivery system AS1411-GO/B3 for tumor targeting. In which, nano- graphene oxide (GO) sheets were employed as drug carrier, and aptamer AS1411 was conjugated onto GO for tumor targeting. The GO also has photothermal effect, which helps the release of B3 from GO as well as thermal cytotoxicity to cells. We found that the release of B3 could response to the acid condition, indicating the tumor intracellular environment could promote the release of B3, thus to perform the chemotherapy effects. This system could also release B3 in responsive to photothermal heating, moreover combined photothermal therapy and chemotherapy to improve the anticancer activity was achieved. This AS1411-GO/B3 platform with chemo-photothermal synergetic therapy provides a very promising treatment for tumor treatment.

Key words: Berberine derivative; Graphene oxide; Near Infrared Ray; Drug release; Chem-photothermal therapy

[View Article Online](#)

[DOI: 10.1039/C9TB02389G](#)

1. Introduction

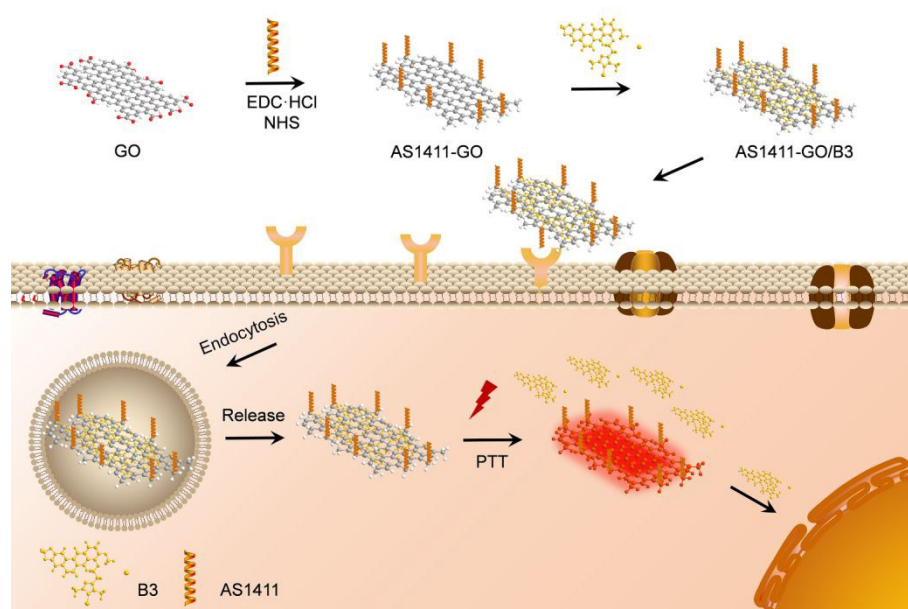
Berberine (BBR), an isoquinoline alkaloid, isolated from traditional Chinese medicine *Coptis chinensis*, which presenting in a variety of plants such as papaveraceae, berberidaceae, ranunculaceae, rhamnaceae and rutaceae¹⁻⁴, has shown many pharmacological activities, such as antibacterial, anti-inflammatory, hypoglycemic, lipid-lowering, antiviral activity etc.⁵⁻⁷ In recent years, the anti-cancer potential of BBR has been reported in many literatures, such as anti-lung cancer, colon cancer, ovarian cancer, bladder cancer and so on.⁸ However, the anticancer activity of BBR is limited.⁹ In order to enhance the anticancer activity of BBR, we previous synthesized a series of BBR derivatives, among which, a novel 9-O-pyrazole alkyl group modified BBR derivative, named B3, has showed significant anti-proliferative activity.¹⁰ However, compound B3 lacks targeting efficiency to tumor, leading to obvious toxic side effects on normal cells. Thus, it is necessary to realize targeting effect via constructing suitable drug delivery system. Moreover, tumor environment responsive drug delivery systems¹¹ and chemo-photothermal synergetic therapy¹²⁻¹⁴ which could release drug on demand to enhanced antitumor efficacy have become increasing attractive.

Graphene oxide (GO), a inorganic nanocarrier, has been applied in the fields of biology and medicine¹⁵, especially drug delivery systems, due to large specific surface area and biocompatibility.^{16, 17} GO has been proven to absorb light and convert it into hyperthermia under 808 nm NIR laser irradiation.¹⁸⁻²¹ This property helps GO to perform photothermal to increase the therapeutic effect.²²⁻²⁴ And the surface of GO contains large numbers of oxygen-containing functional groups, such as carboxyl, amino, and epoxy groups, which facilitate GO link functional groups, such as peptides, proteins, vitamins, polysaccharides, nucleic acids, to achieve functional decoration and improved solubility.^{17, 25} Although GO as a drug carrier has so many advantages, tumor microenvironment and NIR laser dual triggered drug delivery systems have seldom been reported. Designing of drug delivery system with acidic environment responsive drug delivery system will be of great interest.

To realize this, this platform should own the tumor targeting ability. But the targeting effect of GO itself is lacked. It is necessary to endow it with tumor targeting ability. Currently, many tumor-targeting molecules, such as peptides, antibodies, folic acid, and aptamers have been employed as tumor target ligands.²⁶⁻²⁹ Aptamers, a class of oligonucleotides capable of binding to targets with high sensitivity and specificity, have low molecular weight, good chemical stability, ease of modification, adaptability

and no immunogenicity, thus have been applied to biological therapeutics.^{30, 31}

In this work, as shown in Scheme 1, we proposed the design of tumor acidic micro-environment and NIR laser dual responsive drug delivery systems. We further combined the photo-thermal therapy and chemotherapy of B3 together to enhance the therapeutic efficacy. Single strand aptamers targeting to nucleolin named AS1411 aptamers (5'-NH₂-(CH₂)₆GGT GGT GGT GGT TGT GGT GGT GGT GG-3') were connected to the surface of GO by amide reaction to obtain AS1411-GO, the (CH₂)₆ used here is to server as a linker to extend the aptamer from the GO to facilitate the binding of AS1411 with the target molecule. Nucleolin is a multifunctional protein whose main function is to participate in the biological formation of ribosomes.³² Recent studies indicated that nucleolin is overexpressed on various proliferating cancer cell membranes, such as glioma, neuroblastoma, breast cancer, and lung cancer.³²⁻³⁴ The aptamer AS1411 can specifically bind to nucleolin, then endocytosis of the AS1411-GO was mediated by nucleolin to uptake the drug delivery system, thereby achieving active targeting effect.^{26, 35, 36} Furthermore, aptamer with NH₂ terminated can be conjugated to GO. Thus, BBR derivative **B3** with significant anti-cancer activity was adsorbed on the surface of AS1411-GO through π - π conjugate stacking,^{10, 37} and AS1411 was covalent linked to the GO. The AS1411-GO/B3 delivery system is expected to specifically target to nucleolin-overexpressed cancer cells, and achieve chemo-photothermal synergetic therapy.



Scheme 1. Schematic illustration of AS1411-GO/B3 for chemo-photothermal synergetic cancer therapy.

2. Experimental section

2.1 Materials

View Article Online
DOI: 10.1039/C9TB02000A

Berberine chloride was purchased from Lion Biological Technology (Zhengzhou, China). Graphene oxide was purchased from XFNANO (Nanjing, China). The DNA sequences of 5'-NH₂-C₆-GGTGGTGGTGGTTGTGGTGGTGGTGG-3' (underlined part is the AS1411 aptamer, denoted as DNA-AS1411) was purchased from Sangon Biotech (Shanghai, China). N-Hydroxysuccinimide (NHS), 1-ethyl-3-[3-dimethylaminopropyl]-carbodiimide hydrochloride (EDC·HCl) were supplied by Sigma. MTT and porphyrin were supplied by Sangon Biotech (Shanghai, China). Hoechst was supplied by Beyotime Biotechnology (Shanghai, China). Calcein-AM and propidium iodide were purchased from Yeasen Biotech Co., Ltd (Shanghai, China). Pyropheophorbide a (Pyro) was supplied by Shanghai Dibo Biotechnology Co., Ltd. (China). Other solvents and reagents were obtained from Sinopharm Chemical Reagent Co. Ltd.

2.2 Cell lines

A549 cells (human lung adenocarcinoma cell) and L929 cells (mouse fibroblast cell) were purchased from Sangon Biotech (Shanghai, China). A549 cells were cultured in DMEM cell medium including 10% heat-inactivated fetal bovine serum (FBS, BI), 100 µg·mL⁻¹ streptomycin (Hyclone), 100 units·mL⁻¹ penicillin at 37 °C, under 5% CO₂ atmosphere. L929 cells were cultured in RPMI cell medium including 15% heat-inactivated fetal bovine serum (FBS, BI), 100 µg·mL⁻¹ streptomycin (Hyclone), 100 units·mL⁻¹ penicillin at 37 °C, under 5% CO₂ atmosphere.

2.3 Characterization

AFM images were taken on a BRUKER Nano Surface Division (Germany). FT-IR spectra were taken on PerkinElmer L1600300 Spectrum Two Lita (UK). UV spectra were recorded by PERSEE TU-1901 (China). Fluorescence images were obtained on PerkinElmer High Content Analysis System Operetta CLS (HCS, UK). Temperature was monitored by a digital thermometer. Fluorescence spectroscopy measurements were carried out on microplate multimode reader (Thermo Scientific, American). Flow cytometry was analyzed via BD ACCURI C6 PLUS (US). ¹H NMR spectra were taken in a Bruker Avance III 400MHz spectrometer using tetramethylsilane (TMS) as an internal standard. ¹³C NMR spectra were taken in a Bruker Avance III

600MHz spectrometer. The mass spectra were acquired on a Bruker compact Q-TOF (Germany).

View Article Online
DOI: 10.1039/D0TB00489H

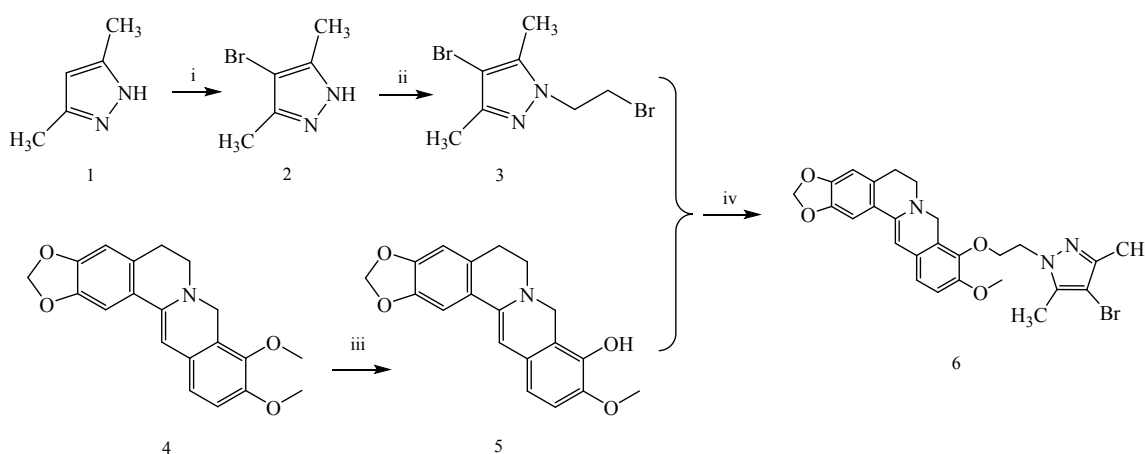
2.4 Synthesis of BBR derivatives

2.4.1 Preparation of compound 3

Compound **3** was prepared according to the improved method in the literature.³⁸ Compound **2** and compound **5** (berberrubine) were synthesized according to the reported methods.³⁹ As shown in Scheme 2, Compound **2** (10 mmol), 1,2-dibromoethane (50 mmol), 40% aq. NaOH solution (0.9 mL), and benzyl triethylammonium chloride (TEBAC) (0.12 g, 0.52 mmol) was mixed and heated at 80 °C with vigorous stirring for 4 h. After the mixture was cooled to room temperature, water (30 mL) was added and extracted the mixture with dichloromethane (3×20 mL), then Mg₂SO₄ was added to dry the extract. The volume of the supernatant was reduced by evaporation under reduced pressure and chromatographed by a silica gel column with dichloromethane/petroleum ether (1/3, v/v) as eluent to obtain compound **3**.

2.4.2 Preparation of B3

A mixture of compound **3** (1.2 mmol), berberrubine (1 mmol), CH₃CN (15 mL), K₂CO₃ (6 mmol) was stirred and heated at 65 °C in reflux for 12 h.¹⁰ Thin layer chromatography (TLC) was used to monitor the progress of the reaction. Then the reaction product was purified by chromatographic separation on a neutral Al₂O₃ column with increasing concentration of ethanol in dichloromethane (CH₂Cl₂/EtOH, 40-24:1, v/v). The final product is **B3**.



Scheme 2. Synthesis of BBR derivate: (i) CH₂Cl₂, NBS, 37 °C, 12 h; (ii) Br(CH₂)₂Br, TEBAC, 40% aq. NaOH, 80 °C, 4 h; (iii) 190 °C, 20-30 mmHg, 30 min; (iv) CH₃CN, K₂CO₃, 12 h.

2.5 The conjugation of AS1411 with GO

Firstly, the nano graphene oxide was prepared from large sized GO. In brief, the mixture of graphene oxide (1 mg/mL) and H₂O₂ (30%) was transferred to a polytetrafluoroethylene (Teflon)-linked autoclave (30 mL) and heated at 162 °C for 20 min and then at 170 °C for 23 min. The resulting solution was then lyophilized to obtain purified small size GO nanosheet, the morphology was observed with AFM microscopy.

AS1411 was covalently connected to GO by the formation of amido bond between the -NH₂ group of the aptamer and the -COOH group of GO by EDC-NHS chemistry.⁴⁰ Firstly, the -COOH group in GO was activated by using EDC (1.5 mmol) and NHS (1.5 mmol) in 6 mL MES (pH 4.6), then stirred for 40 min with sonication. Then, GO was collected by centrifugation and dispersing in 6 mL Tris (pH 7.2). After that, 120 μL of AS1411 was added into GO solution and stirred for 30 min at 25 °C. AS1411-GO was collected by centrifugation and dried in vacuum for further characterization and usage, the conjugation was confirmed by FT-IR spectra and UV spectra. The morphology was observed with AFM microscopy.

2.6 B3 Loading in AS1411-GO

The loading of B3 in AS1411-GO was achieved by mixing drug solution (3 mg·mL⁻¹, in DMSO) and AS1411-GO (1 mg·mL⁻¹). The mixture was stirred in the dark for 12 h at 25 °C, then the B3 loaded AS1411-GO was washed for three times with water to remove the free drug and collected by centrifugation with 13000 rpm at room temperature for 15 min.⁴⁰ The drug loaded AS1411-GO was re-suspended and stored in 4 °C. The drug content of the supernatant was measured by ultraviolet-visible (UV-vis) spectrometry. The loading capacity of AS1411-GO was calculated as follows:

$$\text{The loading capacity (\%)} = \frac{\text{Weight of initial drug} - \text{Weight of supernatant drug}}{\text{Weight of drug loaded nanosheets}} \times 100\%$$

2.7 Drug release behaviors of AS1411-GO/B3

The release behavior of B3 was evaluated in PBS with pH 5.3 and pH 7.4. AS1411-GO/B3 was dispersed in 1 mL PBS. After 30 seconds vortexing, AS1411-GO/B3 was added into a dialysis bag with molecular weight cutoff of 12000 Da immediately and dialysed in 90 mL PBS. The solution was kept constant stirring at 37 °C. At each predetermined interval, 1 mL PBS was taken

out, then 1 mL fresh PBS was added to keep the dialysis volume unchanged. The absorbance value of B3 was measured by UV-visible spectrophotometer at 349 nm. The standard curve for B3 was established by measuring the absorbance values of a series of fixed concentrations of B3. Then B3 content was calculated according to the standard curve and absorbance value. The formula for calculating the cumulative release of drugs is as follows:

$$\text{Percentage of B3 cumulative release (\%)} = \frac{\text{Weight of B3 cumulative release}}{\text{Weight of B3 loaded}} \times 100\%$$

2.8 Near infrared radiation and temperature measurement

To detect the photothermal effect of AS1411-GO/B3, AS1411-GO/B3 at 32 $\mu\text{g}\cdot\text{mL}^{-1}$, 64 $\mu\text{g}\cdot\text{mL}^{-1}$, or 128 $\mu\text{g}\cdot\text{mL}^{-1}$ was dispersed in cell culture medium and loaded in a centrifuge tube, after irradiated for 3 min under 808 nm NIR laser irradiation (2.5 $\text{W}\cdot\text{cm}^{-2}$), the temperature was recorded with a digital thermometer every minute. PBS was set as a control group.

To test the photothermal stability of AS1411-GO/B3, AS1411-GO/B3 at 128 $\mu\text{g}\cdot\text{mL}^{-1}$ was loaded in a centrifuge tube, and irradiated for 3 min under 808 nm NIR laser irradiation with a power density of 2.5 $\text{W}\cdot\text{cm}^{-2}$. Then NIR laser irradiation was stopped and temperature was recorded with a digital thermometer every minute until the normal temperature is restored.

2.9 Cancer targeting and internalization

High content analysis

For cell uptake assessment, porphyrin was used as fluorescence tracer. Porphyrins and AS1411-GO were mixed and stirred at a mass ratio of 1:10 at dark and centrifuged to remove the free porphyrin to obtain porphyrin loaded GO (AS1411-GO/Pyro). A549 cells and L929 cells were plated in 96-well plates with a density of 8×10^3 cells per well and cultured for 12 h with complete culture medium, then the culture medium was replaced with fresh culture medium containing AS1411-GO/Pyro or GO/Pyro and further incubated for 1 h. After removing free complexes, fresh culture medium containing hoechst (5 $\mu\text{g}\cdot\text{mL}^{-1}$) was added to stain the nucleus. After incubated for 5 min, the cells were washed with PBS at 37 $^{\circ}\text{C}$. The cell uptake results were observed by high content analysis system.

Flow cytometry analysis

The cellular uptake of AS1411-GO and GO was further studied by flow cytometry. A549 and L929 cells were incubated for 12 h at 1×10^5 cells per well in 24-well plates. The cells were treated with above mentioned AS1411-GO/B3 for 2 h and then the cells were washed with PBS and centrifuged at 1500 rpm for 5 min, then resuspended in 300 μ L PBS. The cells were analyzed via flow cytometry.

2.9 Cytotoxicity assessment

MTT assay

For cytotoxicity analysis, A549 cells and L929 cells were plated in 96-well plates at a density of 1×10^4 cells per well for 12 h with complete culture medium. Then the culture medium was replaced with fresh culture medium containing AS1411-GO/B3 (with B3 equivalent to $128 \mu\text{g}\cdot\text{mL}^{-1}$) and incubated for 2 h. Then, the AS1411-GO/B3 was removed, the cells were washed with PBS and further incubated for 22 h.

To detect the therapeutic effect of photothermal therapy combined with chemotherapy, A549 cells were plated in 96-well plates with density of 1×10^5 cells per well for 12 h with complete culture medium, then the culture medium was replaced with fresh culture medium (100 μ L) containing AS1411-GO/B3 (with B3 equivalent to $128 \mu\text{g}\cdot\text{mL}^{-1}$) and incubated for 2 h. Then A549 cells were irradiated by 808 nm near-infrared light for 3 min ($2.5 \text{ W}\cdot\text{cm}^{-2}$). Then the AS1411-GO/B3 were removed, and the cells were washed with PBS and further incubated for 22 h.

MTT assay was carried out to measure the cell viability. As mentioned above, after incubation for 22 h, culture medium was replaced by fresh culture medium concluding MTT (100 μ L, $0.5 \text{ mg}\cdot\text{mL}^{-1}$) and incubated for 4 h. After the MTT was removed, DMSO (150 μ L) was added to dissolve the blue crystal. Absorbance at 490 nm was measured by microplate reader.

Calcein-AM/PI double staining experiment

To investigate the therapeutic efficacy of AS1411-GO/B3, Calcein-AM/PI double staining experiment was carried out. In brief, A549 cells and L929 cells were cultured for 24 h. Then the medium was substituted by 100 μ L of fresh medium containing: (1) GO, (2) AS1411-GO, (3) GO/B3, (5) AS1411-GO/B3, (6) AS1411-GO/B3 with NIR laser irradiation, the concentration of B3 was equivalent to $128 \mu\text{g mL}^{-1}$. The cells were incubated with AS1411-GO/B3 for 2 h, and the cells in group (6) were treated with NIR laser irradiation (808 nm, $2.5 \text{ W}\cdot\text{cm}^{-2}$) for 3 min. Then the medium was substituted by 100 μ L of Calcein-AM/PI containing buffer

(2 μM and 1.5 μM , respectively) and the cells were incubated for 15 min to ensure adequate staining. The fluorescence of cells was imaged by high content analysis system, then the number of different cells were counted by Image J software.

View Article Online
DOI: 10.1039/D0TB00489H

3. Results and discussions

3.1 Characterization of B3

The relevant characterizations of B3 are shown in Figure S1, S2 and S3, the results are as follows: ^1H NMR (400 MHz, DMSO) δ 9.56 (s, 1H), 8.93 (s, 1H), 8.17 (d, $J = 9.2$ Hz, 1H), 7.98 (d, $J = 9.0$ Hz, 1H), 7.79 (s, 1H), 7.10 (s, 1H), 6.18 (s, 2H), 4.85 (t, $J = 8.0$ Hz, 2H), 4.65 (t, $J = 5.1$ Hz, 2H), 4.52 (t, $J = 5.2$ Hz, 2H), 4.02 (s, 3H), 3.22 (t, $J = 7.5$ Hz, 2H), 2.25 (s, 3H), 2.03 (s, 3H). ^{13}C NMR (101 MHz, DMSO) δ 150.58, 150.36, 148.21, 145.62, 145.11, 142.57, 138.31, 137.91, 133.26, 131.02, 127.01, 124.08, 121.95, 120.85, 120.61, 108.93, 105.91, 102.59, 93.29, 72.31, 57.41, 55.85, 49.79, 26.85, 12.41, 10.43. HRMS (ESI⁺): m/z for $\text{C}_{26}\text{H}_{25}\text{BrN}_3\text{O}_4^+ [\text{M}-\text{Br}]^+$ calcd 524.1006, found 524.1113. These results all indicated the B3 has been successfully synthesized.

3.2 Characterization of AS1411-GO/B3 nanosheets

Before B3 was loaded in GO, AS1411 was covalently attached to GO by EDC-NHS chemistry. The FTIR spectroscopy (Figure 1A) indicated that AS1411 was successfully connected to GO (Figure 1A). The characteristic absorption peaks of GO including telescopic vibration of O-H (~ 3470 cm^{-1}), stretching vibration of C=O in carboxyl groups (~ 1724 cm^{-1}), telescopic vibration of C=C (~ 1635 cm^{-1}), telescopic vibration of C-O in ether bonds (~ 1074 cm^{-1}), in-plane bending vibration of O-H (~ 1394 cm^{-1}).⁴⁰⁻⁴²

FTIR spectroscopy showed that AS1411 and GO were connected successfully and the amide bond was formed. The peak of the amide bond appears, including the amide peak I, stretching vibration of C=O (~ 1640 cm^{-1}), the amide peak II, bending vibration of N-H (~ 1570 cm^{-1}), the amide peak III, stretching vibration of C-N (~ 1380 cm^{-1}).⁴³ The characteristic peak also includes $-\text{CH}_2-$ (~ 2920 cm^{-1} and ~ 2980 cm^{-1}) of AS1411. The disappearance of stretching vibration of C=O in carboxyl groups (~ 1724 cm^{-1}) was also observed.

FTIR spectroscopy showed that the characteristic peaks of B3 including telescopic vibration of C-H bonds on benzene rings

($\sim 3031\text{ cm}^{-1}$), telescopic vibration of C-H bonds in methyl ($\sim 2945\text{ cm}^{-1}$), stretching vibration of C=C in benzene ring ($\sim 1605\text{ cm}^{-1}$), bending vibration of C-N ($\sim 1402\text{ cm}^{-1}$), stretching vibration of C-N ($\sim 1338\text{ cm}^{-1}$), telescopic vibration of C-C bond in benzyl group ($\sim 1105\text{ cm}^{-1}$). FTIR spectroscopy of AS1411-GO/B3 showed telescopic vibration of C-H bonds in methyl ($\sim 2945\text{ cm}^{-1}$), a specific bond in B3, stretching vibration of C=O in amide bond ($\sim 1640\text{ cm}^{-1}$), and characteristic peaks of amide bond,¹⁰ indicating the B3 has been loaded in the AS1411-GO.

The results were further proved by UV-vis spectra (Figure 1B). The characteristic absorption peaks of free GO, AS1411, B3 were $\sim 230\text{ nm}$, $\sim 258\text{ nm}$, $\sim 348\text{ nm}$, respectively. After AS1411 was connected to GO, AS1411-GO had a new absorption shoulder at $\sim 258\text{ nm}$.^{44, 45} Compared to free B3, AS1411-GO/B3 displayed a new absorption shoulder at $\sim 230\text{ nm}$, and the absorption peak at $\sim 260\text{ nm}$ of B3 has been red-shifted to $\sim 262\text{ nm}$, which could be attributed to the ground-state electron donor-acceptor interaction between GO and B3.⁴⁰ UV data were further confirmed by fluorescence characterization (Figure 1C). In fluorescence spectrum, free B3 exhibits a fluorescence excitation maximum at $\sim 470\text{ nm}$ and emission maximum at $\sim 553\text{ nm}$. After B3 was absorbed to AS1411-GO, AS1411-GO/B3 exhibit significant quenching of $\sim 553\text{ nm}$ emission with excitation wavelength of $\sim 470\text{ nm}$.⁴⁶ This phenomenon indicates the existence of π - π conjugate stacking between AS1411-GO and B3, causing the decay of excitons through GO.⁴⁷

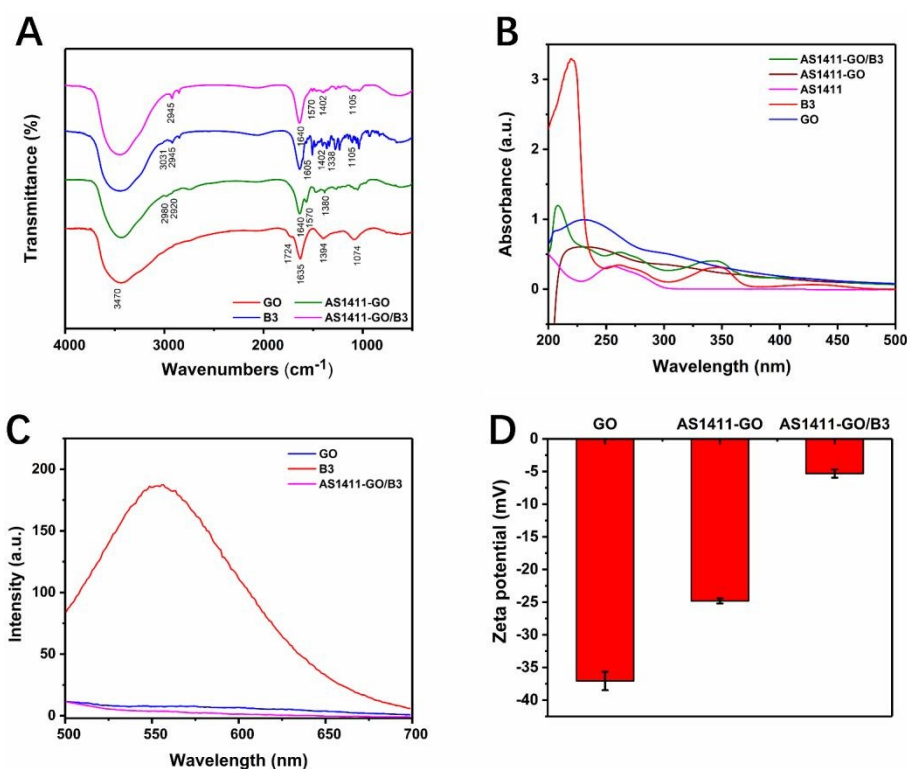


Figure 1. (A) FTIR spectra of GO, AS1411-GO, free B3, AS1411-GO/B3. (B) UV-vis spectra of GO, free AS1411, free B3,

AS1411-GO, and AS1411-GO/B3. (C) Fluorescence spectra of GO, free B3, and AS1411-GO/B3. (D) Zeta potential of GO, AS1411-GO, and AS1411-GO/B3.

View Article Online
DOI: 10.1039/D0TB00489H

The morphology of AS1411-GO/B3 was characterized by atomic force microscopy (AFM). The results (Figure 2) indicated the size of GO (Figure 2A), AS1411-GO (Figure 2B) and AS1411-GO/B3 (Figure 2C) were around 30-50 nm and the thickness of GO, AS1411-GO and AS1411-GO/B3 were 0.8-1 nm, 1.5-2 nm, 2-3 nm, respectively, the increased thickness may be attributed to the modification of AS1411 and B3 on GO. The small size of these nanosheets may facilitate their cellular uptake. The zeta potential was also measured. As shown in Figure 1D, the zeta potential of GO was -37.07 ± 1.40 mV, which could be attributed to the carboxyl groups on the surface of GO. After conjugation with AS1411, the potential value changed to -24.83 ± 0.38 mV. Furthermore, the loading of positively charged B3 resulted a change in the zeta potential to -5.32 ± 0.63 mV.

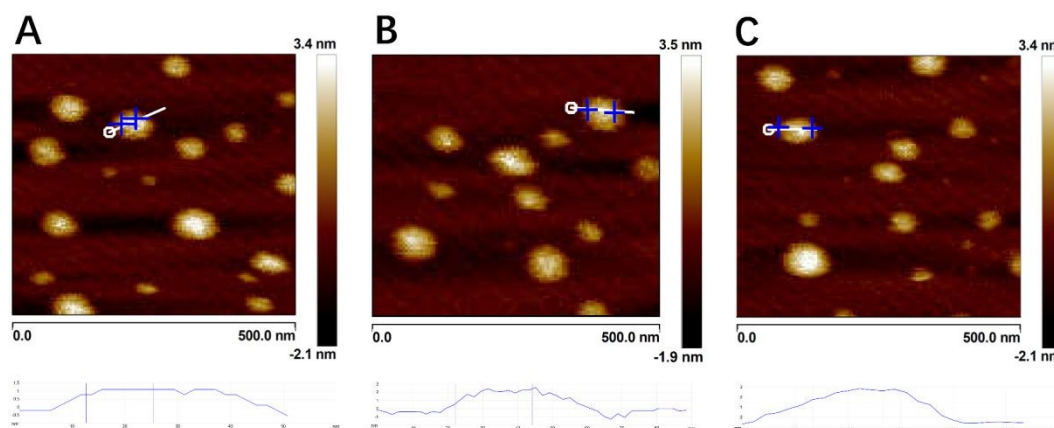


Figure 2. AFM images of (A) GO (B) AS1411-GO and (C) AS1411-GO/B3.

3.3 Drug loading capacity of AS1411-GO/B3 nanosheets

The relationship between the drug loading capacity and the initial B3 concentration was investigated (Figure 3A). With the initial B3 concentration increased, the loading capacity of AS1411-GO increased gradually. When the initial B3 concentration reached 3 mg mL^{-1} , the growth rate of loading capacity was slowed down. The saturated loading capacity was 68.63% with an initial B3 concentration being 3.5 mg mL^{-1} . This result indicated that the loading capacity of AS1411-GO is high. Single-layer GO has an aromatic structure on both sides, which enables it to absorb aromatic compounds with similar structures. The large specific surface area of GO and the large π - π stacking of GO and B3 make it has high drug-loading capacity.⁴⁸ We also studied the effect of environmental pH on loading capacity (Figure 3B). The experiments were conducted with an initial B3 concentration of 1 mg mL^{-1} .

mL^{-1} at pH 5.6, 7.4, or 9.0. As the results shown, the solution pH has no significant effect on loading capacity. With the increase of ambient pH, the drug loading capacity increased slightly. The loading capacity was 44.31%, 45.48%, 46.73% at pH 5.6, 7.4, 9.0, respectively.

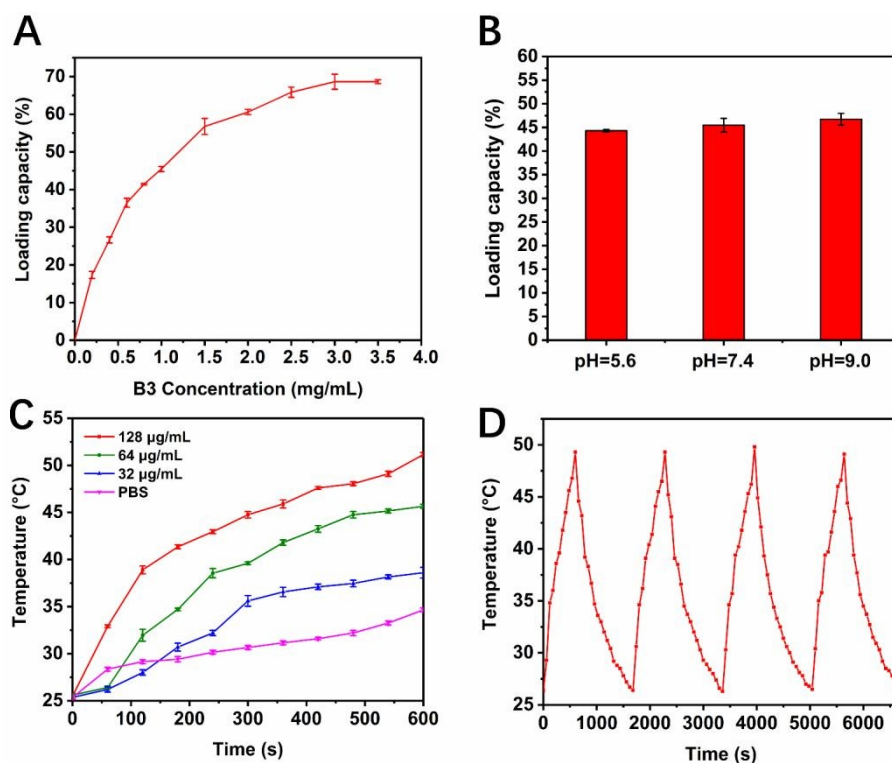


Figure 3. (A) The effect of initial B3 concentration on the loading capacity. The concentration of AS1411-GO was kept at $1 \text{ mg}\cdot\text{mL}^{-1}$. (B) The effect of solution pH on the loading capacity. The initial B3 concentration is $1 \text{ mg}\cdot\text{mL}^{-1}$. (C) The change curve of temperature of AS1411-GO/B3 with various concentrations under the laser irradiation. PBS was used as the control group. (D) Temperature changes in AS1411-GO/B3 aqueous solution ($128 \mu\text{g}\cdot\text{mL}^{-1}$) over four times of power on/off cycles under the laser irradiation.

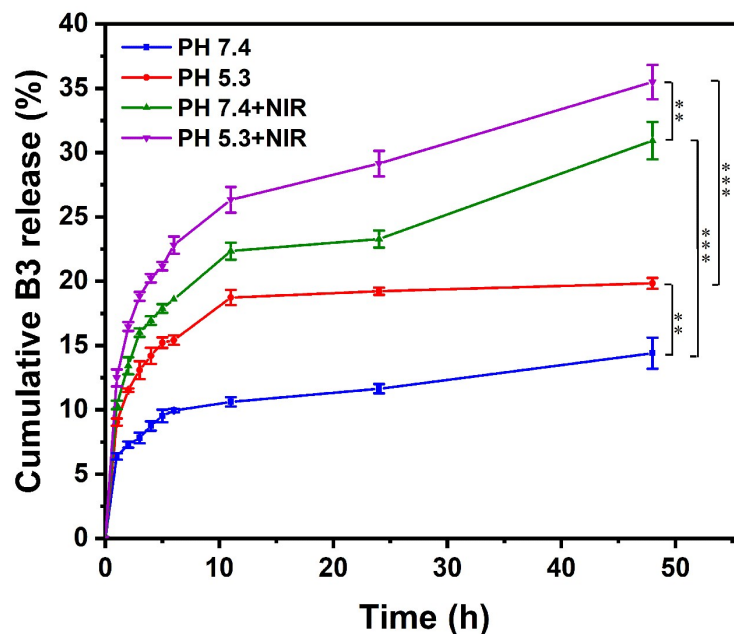
3.4 Photothermal heating effect of AS1411-GO/B3 nanoplatform

In order to study the photothermal properties of AS1411-GO/B3, different concentrations of AS1411-GO/B3 were irradiated under 808 nm NIR laser irradiation ($2.5 \text{ W}\cdot\text{cm}^{-2}$) for 3 min, then the temperature variation was recorded by a digital thermometer, while an PBS buffer solution was set as a negative control. As illustrated in Figure 3C, with the increase of the irradiation time, the temperature of the drug increases gradually. When the NIR laser irradiation time reaches 10 min, the temperature of AS1411-GO/B3 with a concentration of $128 \mu\text{g}\cdot\text{mL}^{-1}$ achieved 51.2°C and the temperature increased by 25.6°C , whereas the PBS

only respond to NIR laser irradiation slightly. The concentration-dependent temperature change was observed obviously in the Figure 3C, compared with AS1411-GO/B3 at 128 $\mu\text{g}\cdot\text{mL}^{-1}$, the temperature of AS1411-GO/B3 at 32 $\mu\text{g}\cdot\text{mL}^{-1}$ for 600 s only achieved 38.6 °C. Furthermore, negligible change in photothermal conversion was observed after four cycles of 808 nm NIR laser irradiation ($2.5\text{ W}\cdot\text{cm}^{-2}$) for 3 min. The results indicated AS1411-GO/B3 possessed a splendid photothermal conversion ability reliable photothermal stability, which is beneficial to photothermal therapy of cancer.

3.5 Drug release behavior of AS1411-GO/B3 nanosheets

The B3 release kinetics in PBS under simulated normal physiological environment (pH 7.4) and simulated tumor environment (pH 5.3) together with or without NIR laser irradiation were studied. (Figure 3D) The characteristics of B3 release from AS1411-GO/B3 in different environments were compared. The pH of tumor tissues is lower than normal tissues because tumor cells metabolize differently from normal cells and metabolism produced more lactic acid.⁴⁹ As illustrated in Figure 4, AS1411-GO/B3 showed a burst release of B3 at the beginning, then gradually slowed down after 6 h. Obviously, the cumulative release of B3 in acidic pH is 18% after 48 hours dialysis, which is significantly higher than the cumulative release in physiological pH being 12%. The phenomenon indicated that the drug release of AS1411-GO/B3 in the normal physiological environment, such as blood stream, is slow, while in acidic condition, the release will accelerate. Under NIR laser irradiation, the cumulative drug release of B3 in acidic environment and normal physiological environment increased to 35% and 31%, respectively. And the cumulative drug release was significantly improved compared to no irradiation. The results indicate that **B3** release rate was stimulated by NIR laser irradiation, which means **B3** release property can be controlled by external signal. All data demonstrate the intelligent dual-stimuli-response property of AS1411-GO/B3.²⁴



View Article Online
DOI: 10.1039/D0TB00489H

Figure 4. B3 release profiles from AS1411-GO/B3 at different pH levels with or without NIR laser irradiation (808 nm, 2.5 W·cm⁻²) (**P < 0.01, ***P < 0.001).

3.6 Targeting ability evaluation of nanosheet based on cellular uptake

To study the targeting performance of AS1411-GO drug delivery nanoplatform, porphyrin was selected as a biotracer.⁵⁰ A549 cells were used as positive cells, whereas L929 cells were used as negative controls. The high content analysis results were shown in Figure 5, which indicate that A549 cells incubated with AS1411-GO/pyro exhibited a stronger red fluorescence compared to the A549 cells treated with non-targeting GO/pyro. However, L929 cells (Figure 5), show a weak red fluorescence regardless of AS1411-GO/pyro or non-targeting GO/pyro, which implying that AS1411-GO had none specific binding to negative cells. The results indicate that active targeting of AS1411-GO was achieved by AS1411, which could specifically bind to nucleolin proteins overexpressed on the surface of A549 cells. The active targeting of AS1411-GO is beneficial to increase the accumulation of AS1411-GO/B3 in tumor tissues and reduce the side effects on normal cells.²⁶

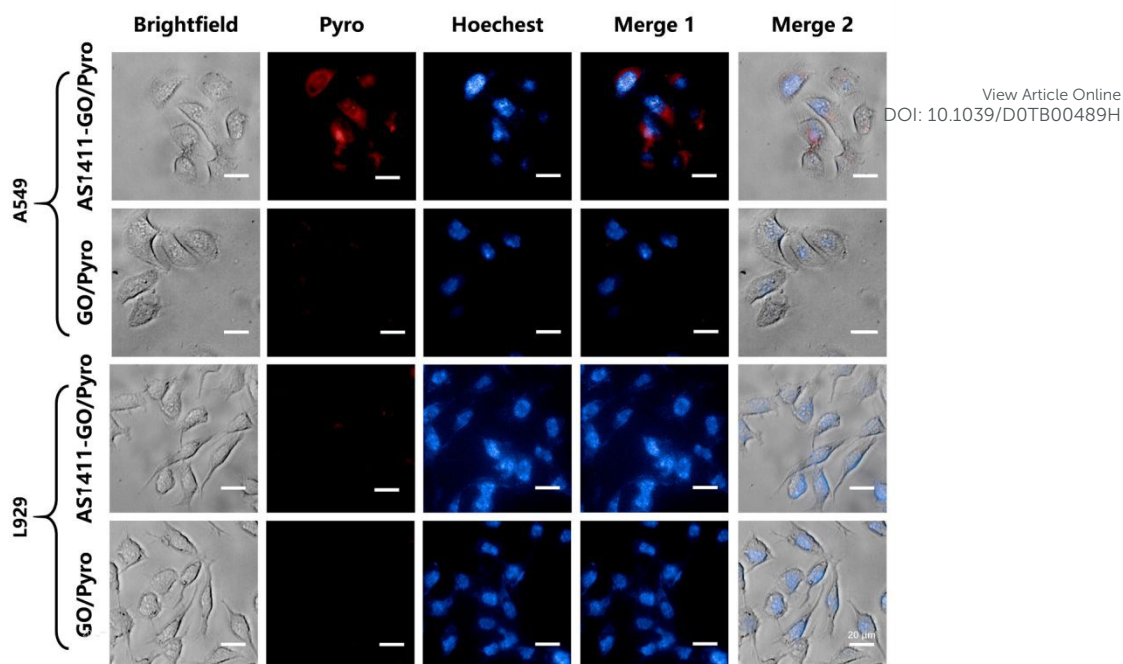


Figure 5. High content images of A549 cells and L929 cells after incubation with AS1411-GO/pyro ($128 \mu\text{g}\cdot\text{mL}^{-1}$) and GO/pyro ($128 \mu\text{g}\cdot\text{mL}^{-1}$). Cell nucleus were labeled using Hoechst (blue). The red fluorescence in these images come from porphyrin.

The targeting performance of AS1411-GO drug delivery nanoplatform was further confirmed by flow cytometry. As shown in Figure 6, a significant increase of fluorescence intensity from AS1411-GO/Pyro in A549 cells were observed, which was significant stronger than that of the A549 cells incubated with non-targeting GO/Pyro. However, no apparent change was observed between AS1411-GO/Pyro and GO/Pyro when incubated with L929 cells (control), implying that the AS1411-GO/Pyro had no selectivity to cancer cells and there are some none specific binding to the negative cells.

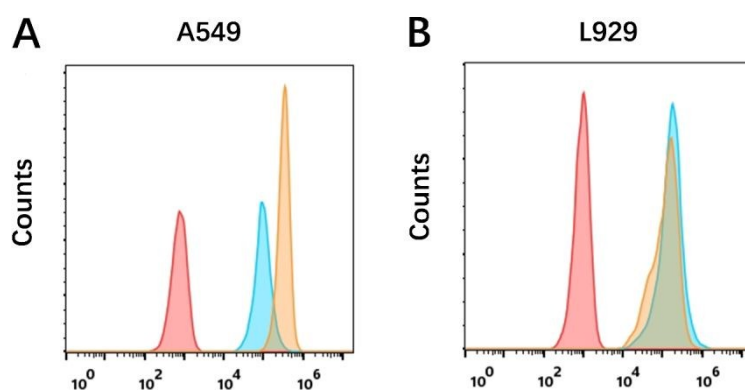


Figure 6. Flow cytometry histogram of A549 cells (A) and L929 cells (B) after treatment with GO/Pyro (blue), AS1411-GO/Pyro (yellow) and without treatment (red).

3.7 Synergetic therapeutic efficacy evaluated using MTT assay and Calcein-AM/PI double staining assay

The therapeutic effect and biocompatibility of the drug delivery system are crucial to the biomedical application. ^{View Article Online} In this work, A549 cells and L929 cells were treated with various formulations and determined with MTT for cytotoxicity analysis. As Figure 7A and Figure 7B shown, when the concentration of GO and AS1411-GO reached $128 \mu\text{g}\cdot\text{mL}^{-1}$, the cells survival rate of A549 cells and L929 cells are still around 98%, indicating GO and AS1411-GO has almost no cytotoxicity. A549 cells were further incubated with different concentration of GO/B3 and AS1411-GO/B3 to investigate the therapeutic efficiency. As demonstrated in Figure 7, with the increase of GO/B3 concentration, the chemotherapy effect of GO/B3 increases slightly, and the survival rate of A549 cells was decreased to about 81% at concentration of $128 \mu\text{g}\cdot\text{mL}^{-1}$. Whereas the survival rate of A549 cells was drastically decreased to about 51% when treated with the same concentration of AS1411-GO/B3. While the survival rate of L929 cells was decreased only to 68%, indicating that AS1411-GO/B3 showed weaker cytotoxicity to negative L929 cells. Because there are much lower nucleolin proteins on the surface of L929 cells. AS1411-GO/B3 was favor to accumulated in the A549 cells, increasing anti-tumor effect.⁵¹ These results illustrate the targeted therapeutic effect of AS1411-GO/B3.

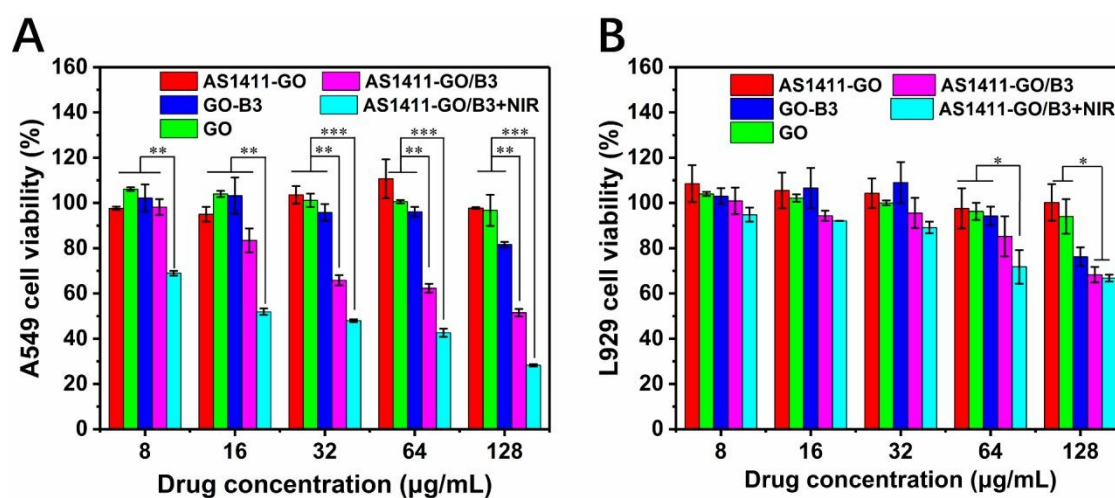


Figure 7. Cell viability of A549 cells (A) and L929 cells (B) treated with various concentrations of GO, AS1411-GO, GO/B3, and AS1411-GO/B3 with or without NIR laser irradiation (* $P < 0.05$, ** $P < 0.01$, *** $P < 0.001$).

To further improve the therapeutic efficiency, chemotherapy combined with photothermal therapy were carried out. Under 808 nm NIR laser irradiation ($2.5 \text{ W}\cdot\text{cm}^{-2}$, 3 min), the therapeutic effect of AS1411-GO/B3 was enhanced significantly, and the survival rate of A549 cells reduced from 51% (without NIR) to 28%. Compared to the only chemotherapy groups (without NIR),

significantly lower viability of A549 cells was observed, while in L929 cells, only in high dose groups, the NIR treatment further caused some increase in the cytotoxicity, while the effects has significantly increase in all the doses tested, which indicated that targeting drug delivery and chemo-photothermal synergetic therapy has enhanced the therapeutic effect.

Cell viability was also analyzed by the calcein-AM/propidium iodide (PI) double staining. Calcein-AM is an excellent staining reagent for fluorescent labeling of living cells, which can easily penetrate the membrane of living cells and emit green fluorescence. Propidium iodide (PI) can only enter dead cells and bind with nucleic acids to produce fluorescent signal. By comparing the ratio of red and green fluorescent cells, we can observe the therapeutic efficacy between different groups. As shown in Figure 8 and Table S1, GO and AS1411-GO has almost no cytotoxicity to A549 cells and L929 cells. For untreated A549 cells and L929 cells, with the NIR light irradiation for 3 min did not decrease cell viability (Figure 5A). In the case of treated positive A549 cells, the GO/B3 group exhibited fluorescence, which confirmed that GO/B3 would cause obvious damage on A549 cells. Then we compared the cells treated by GO/B3 and AS1411-GO/B3. The statistical results indicate that the ratio of cells stained by PI to total cells in AS1411-GO/B3 treated group (0.3274) was significantly higher than GO/B3 treated group (0.2466), which could be attributed to the active targeting of AS1411.⁵² In AS1411-GO/B3 group, the ratio of red-stained cells reached to 0.6895, which may be due to the photothermal effect of GO under NIR laser irradiation. In terms of negative L929 cells, there is no obvious difference in the ratio of red-stained cells in GO/B3 treated group and AS1411-GO/B3 treated group.

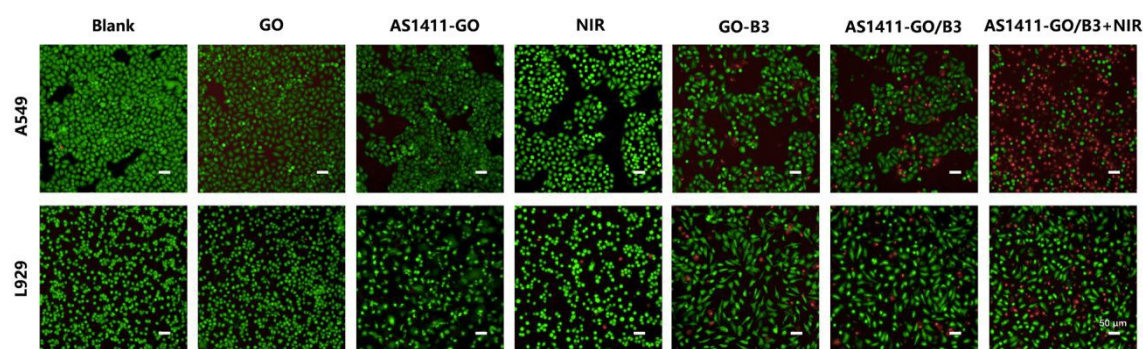


Figure 8. Calcein-AM/PI double staining experiment on A549 cells and L929 cells under the treatment of GO, AS1411-GO, only NIR laser irradiation, GO/B3, AS1411-GO/B3, and AS1411-GO/B3 with NIR laser irradiation.

4. Conclusion

In summary, acidic tumor microenvironment condition and NIR laser dual responsive of novel chemotherapy drug BBR

derivative B3 loaded in GO was successfully constructed for targeted and synergetic treatment of cancer cells. The active targeting molecular AS1411 aptamer performed as an active targeting ligand to mediate the uptake of drug delivery system AS1411-GO/B3. The prepared nanosheets can enter nucleolin-positive cancer cells with high efficiency. B3 can be released into cancer cells by the stimuli of the acidic environment and the external NIR laser irradiation, thus enhancing the efficiency of chemotherapy. The nanoplateforms possessed remarkable photothermal conversion ability. High anti-tumor efficiency of drug delivery system was achieved by the combination both photothermal therapy and chemotherapy. Overall, the constructed drug delivery system provided a promising and attractive strategy for potential treatment of cancer.

ACKNOWLEDGMENTS

We gratefully acknowledge the financial support from the Huxiang Young Talent Program of Hunan Province (2018RS3005), the Project of Innovation-driven Plan in Central South University (2020CX048), the Natural Science Foundation of Hunan Province, China (2019JJ60071), the Shenghua Yuying Project of Central South University, the Postgraduate Innovation Project of Central South University (2019zzts449, 2019zzts750, 2019zzts1017), the Hunan Provincial Graduate Research and Innovation Project (CX20190184, CX20190242), and the Key Research Fund of Hunan Provincial Education Department (18A211).

References

1. I. P. Singh and S. Mahajan, *Expert Opin. Ther. Patents*, 2013, **23**, 215-231.
2. E. Mirhadi, M. Rezaee and B. Malaekhehnikouei, *Biomedical Chromatography BMC*, 2018, **1060**, e4279.
3. J. Tabeshpour, M. Imenshahidi and H. Hosseinzadeh, *Iranian Journal of Basic Medical Sciences*, 2017, **20**, 557-568.
4. M. Imanshahidi and H. Hosseinzadeh, *Phytotherapy Research*, 2008, **22**, 999-1012.
5. E. Kupeli, M. Kosar, E. Yesilada, K. Husnu and K. H. C. Baser, *Life Sciences*, 2002, **72**, 645-657.
6. H. Luo, C. T. Vong, H. B. Chen, Y. Gao, P. Lyu, L. Qiu, M. M. Zhao, Q. Liu, Z. H. Cheng, J. Zou, P. F. Yao, C. F. Gao, J. C. Wei, C. O. L. Ung, S. P. Wang, Z. F. Zhong and Y. T. Wang, *Chin. Med.*, 2019, **14**, 58.
7. K. Hayashi, K. Minoda, Y. Nagaoka, T. Hayashi and S. Uesato, *Bioorganic & Medicinal Chemistry Letters*, 2007, **17**, 1562-1564.
8. J. H. Xu, Y. M. Long, L. W. Ni, X. Y. Yuan, N. Yu, R. H. Wu, J. L. Tao and Y. S. Zhang, *BMC Cancer*, 2019, **19**, 20.
9. M. U. K. Sahibzada, A. Sadiq, H. S. Faidah, M. Khurram, M. U. Amin, A. Haseeb and M. Kakar, *Drug Des. Dev. Ther.*, 2018, **12**, 303-312.
10. D. Xiao, F. He, D. Peng, J. Peng, M. Zou, Y. Liu and Z. Liu, *Anti-cancer agents in medicinal chemistry*, 2018, DOI: 10.2174/1871520618666180717121208.
11. F. He, N. Wen, D. Xiao, J. Yan, H. Xiong, S. Cai, Z. Liu and Y. Liu, *Curr Med Chem*, 2018, DOI:

- 10.2174/0929867325666181008142831.
12. W. Cheng, X. Zeng, H. Chen, Z. Li, W. Zeng, L. Mei and Y. Zhao, *ACS Nano*, 2019, **13**, 8537-8565.
13. X. Zeng, M. Luo, G. Liu, X. Wang, W. Tao, Y. Lin, X. Ji, L. Nie and L. Mei, *Adv Sci (Weinh)*, 2018, **5**, 1800510. View Article Online
DOI: 10.1039/D0TB00489H
14. W. Cheng, J. Nie, N. Gao, G. Liu, W. Tao, X. Xiao, L. Jiang, Z. Liu, X. Zeng and L. Mei, *Advanced Functional Materials*, 2017, **27**.
15. Z. Liu, S. Chen, B. Liu, J. Wu, Y. Zhou, L. He, J. Ding and J. Liu, *Anal Chem*, 2014, **86**, 12229-12235.
16. J. Zhang, L. Song, Z. Zhang, N. Chen and L. Qu, *Small*, 2014, **10**, 2151-2164.
17. N. Duran, D. S. T. Martinez, C. P. Silveira, M. Duran, A. C. M. de Moraes, M. B. Simoes, O. L. Alves and W. J. Favaro, *Current Topics in Medicinal Chemistry*, 2015, **15**, 309-327.
18. B. Tian, C. Wang, S. Zhang, L. Feng and Z. Liu, *Acs Nano*, 2011, **5**, 7000-7009.
19. J. T. Robinson, S. M. Tabakman, Y. Liang, H. Wang, H. S. Casalongue, V. Daniel and H. Dai, *Journal of the American Chemical Society*, 2011, **133**, 6825-6831.
20. N. Mauro, A. L. Volsi, C. Scialabba, M. Licciardi, G. Cavallaro and G. Giammona, *Curr. Drug Deliv.*, 2017, **14**, 433-443.
21. M. J. Gao, S. S. Lv, J. X. Qiu, W. Du, X. T. Zhang, X. C. He, X. M. Li, X. F. Ma and G. Li, *GO/DNA/Au/PANi Nanocomposite with High Photoconductive Responses to Visible Light and NIR*, Springer-Verlag Singapore Pte Ltd, Singapore, 2018.
22. H. B. Zhang, Y. Li, Z. Pan, Y. L. Chen, Z. X. Fan, H. N. Tian, S. Zhou, Y. B. Zhang, J. J. Shang, B. L. Jiang, F. F. Wang, F. H. Luo and Z. Q. Hou, *Mol. Pharm.*, 2019, **16**, 1982-1998.
23. C. Z. Huang, X. Hu, Z. S. Hou, J. B. Ji, Z. H. Li and Y. X. Luan, *J. Colloid Interface Sci.*, 2019, **545**, 172-183.
24. R. Sang, M. Chen, Y. Y. Yang, Y. F. Li, J. C. Shi, Y. Deng, X. C. Chen and W. Z. Yang, *Journal of Biomedical Materials Research Part A*, 2019, **107**, 2296-2309.
25. S. Y. Wu, S. S. A. An and J. Hulme, *International Journal of Nanomedicine*, 2015, **10**, 9-24.
26. L. Y. Jiang, H. Wang and S. Z. Chen, *Journal of Nanoscience and Nanotechnology*, 2020, **20**, 2025-2031.
27. O. Asadpour and F. Rahbarizadeh, *Cell J.*, 2020, **22**, 30-39.
28. G. Y. Wan, Y. Y. Cheng, J. Song, Q. Chen, B. W. Chen, Y. Y. Liu, S. L. Ji, H. L. Chen and Y. S. Wang, *Chem. Eng. J.*, 2020, **380**, 17.
29. N. Mauro, C. Scialabba, S. Agnello, G. Cavallaro and G. Giammona, *Materials science & engineering. C, Materials for biological applications*, 2020, **107**, 110201.
30. C. Zhu, G. Yang, M. Ghulam, L. Li and F. Qu, *Biotechnology advances*, 2019, **37**, 107432.
31. J. Yan, H. Xiong, S. Cai, N. Wen, Q. He, Y. Liu, D. Peng and Z. Liu, *Talanta*, 2019, **200**, 124-144.
32. D. H. M. Dam, J. H. Lee, P. N. Sisco, D. T. Co, M. Zhang, M. R. Wasielewski and T. W. Odom, *Acs Nano*, 2012, **6**, 3318-3326.
33. A. G. Hovanesian, C. Soundaramourty, D. El Khoury, I. Nondier, J. Svab and B. Krust, *Plos One*, 2010, **5**, 13.
34. D. H. M. Dam, R. C. Lee and T. W. Odom, *Nano Letters*, 2014, **14**, 2843-2848.
35. H. Xiong, J. Yan, S. Cai, Q. He, D. Peng, Z. Liu and Y. Liu, *Int J Biol Macromol*, 2019, **132**, 190-202.
36. W. Zhou, Y. Zhou, J. Wu, Z. Liu, H. Zhao, J. Liu and J. Ding, *J Drug Target*, 2014, **22**, 57-66.
37. S. Shim, *Bull. Korean Chem. Soc.*, 2019, **40**, 366-369.
38. O. S. Attarian, S. G. Matsuyan and S. S. Martirosyan, *Khim. Geterotsiklicheskikh Soedin.*, 2005, 533-536.
39. K. Iwasa, M. Kamigauchi, M. Ueki and M. Taniguchi, *Eur. J. Med. Chem.*, 1996, **31**, 469-478.
40. Y. Lu, P. Wu, Y. Yin, H. Zhang and C. Cai, *J. Mater. Chem. B*, 2014, **2**, 3849-3859.
41. H. Y. Liu, P. X. Xi, G. Q. Xie, Y. J. Shi, F. P. Hou, L. Huang, F. J. Chen, Z. Z. Zeng, C. W. Shao and J. Wang, *J. Phys. Chem. C*, 2012, **116**, 3334-3341.
42. H. Kim, D. Lee, J. Kim, T. I. Kim and W. J. Kim, *Acs Nano*, 2013, **7**, 6735-6746.
43. X. L. Wang and Z. X. Wang, *Chem. J. Chin. Univ.-Chin.*, 2018, **39**, 2185-2191.
44. Y. Xu, S. Tan, Q. Liang and M. Ding, *Sensors (Basel)*, 2017, **17**.
45. A. Deb and R. Vimala, *J. Drug Deliv. Sci. Technol.*, 2018, **43**, 333-342.
46. K. Vinothini, N. K. Rajendran, M. A. Munusamy, A. A. Alarfaj and M. Rajan, *Mater. Sci. Eng. C-Mater. Biol. Appl.*, 2019, **100**, 676-687.
47. S. Nandi, A. Kundu and A. K. Nandi, *Journal of Nanoscience & Nanotechnology*, 2016, **16**, 7363-7372.
48. W. Jiang, F. Mo, Y. Lin, X. Wang, L. Xu and F. Fu, *J. Mat. Chem. B*, 2018, **6**, 4360-4367.

49. K. G. de la Cruz-Lopez, L. J. Castro-Munoz, D. O. Reyes-Hernandez, A. Garcia-Carranca and J. Manzo-Merino, *Front. Oncol.*, 2019, **9**, 21.
50. J. Y. Shi, T. W. B. Liu, J. Chen, D. Green, D. Jaffray, B. C. Wilson, F. Wang and G. Zheng, *Theranostics*, 2011, **1**, 363-370. DOI: 10.1039/D0TB00489H
51. K. Saravanakumar, X. Hu, S. Shanmugam, R. Chelliah, P. Sekar, D.-H. Oh, S. Vijayakumar, K. Kathiresan and M.-H. Wang, *Archives of biochemistry and biophysics*, 2019, **671**, 143-151.
52. A. Barzegar Behrooz, F. Nabavizadeh, J. Adiban, M. Shafiee Ardestani, R. Vahabpour, M. R. Aghasadeghi and H. Sohanaki, *Clin Exp Pharmacol Physiol*, 2017, **44**, 41-51.

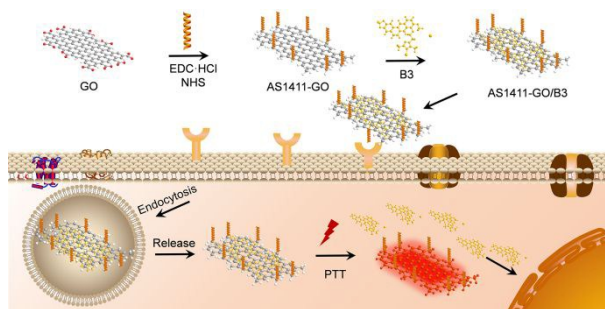


Table of contents entry:

Stimuli responsive release of berberine 9-O-pyrazole alkyl derivative loaded in AS1411 functionalized graphene oxide nanosheets for chemo-photothermal synergetic therapy cancer